

1 **Highlights:**

2

- 3 • insight into geomorphological processes operating on rocky shores in
4 High Arctic

5

- 6 • first use of SilverSHRT and TMEM tests in Svalbard rocky coast
7 geomorphology study

8

- 9 • geophysical (ERT) evidence of the impact of sea on the state of coastal
10 permafrost

11

- 12 • new conceptual model of High Arctic rock coast system

13

14

15 **Cryo-conditioned rocky coast systems: a case study from Wilczekodden, Svalbard**

16 Strzelecki M.C.¹, Kasprzak M.¹, Lim M.², Swirad Z.M.³, Jaskólski M.¹, Pawłowski Ł.¹, Modzel P.¹.

17 *1-Institute of Geography and Regional Development, University of Wrocław, pl. Uniwersytecki 1, 50-137 Wrocław, Poland*

18 *2- Engineering & Environment, Northumbria University, Ellison, Northumberland Road, Newcastle upon Tyne NE1 8ST,*
19 *UK*

20 *3-Department of Geography, Durham University, South Road DH1 3LE, Durham UK*

21

22

23 **Abstract:**

24 *This paper presents the results of an investigation into the processes controlling development of a cryo-*
25 *conditioned rock coast system in Hornsund, Svalbard. A suite of nested geomorphological and geophysical*
26 *methods have been applied to characterize the functioning of rock cliffs and shore platforms influenced by*
27 *lithological control and geomorphic processes driven by polar coast environments. Electrical resistivity*
28 *tomography (ERT) surveys have been used to investigate permafrost control on rock coast dynamics and reveal*
29 *the strong interaction with marine processes in High Arctic coastal settings. Schmidt hammer rock tests,*
30 *demonstrated strong spatial control on the degree of rock weathering (rock strength) along High Arctic rock*
31 *coasts. Elevation controlled geomorphic zones are identified and linked to distinct processes and mechanisms,*
32 *transitioning from peak hardness values at the ice foot through the wave and storm dominated scour zones to*
33 *the lowest values on the cliff tops, where the effects of periglacial weathering dominate. Observations of rock*
34 *surface change using a traversing micro-erosion meter (TMEM) indicate that significant changes in erosion*
35 *rates occur at the junction between the shore platform and the cliff toe, where rock erosion is facilitated by*
36 *frequent wetting and drying and operation of nivation and sea ice processes (formation and melting of snow*
37 *patches and icefoot complexes). The results are synthesised to propose a new conceptual model of High Arctic*
38 *rock coast systems, with the aim of contributing towards a unifying concept of cold region landscape evolution*
39 *and providing direction for future research regarding the state of polar rock coasts.*

40 **Keywords:** rock coast evolution, periglacial processes, cryo-conditioning; coastal

41 **permafrost, Svalbard, High Arctic**

42 **I. Introduction**

43 Since the beginning of the 21st century periglacial researchers have challenged longstanding
44 theoretical concepts of landscape evolution in cold environments (e.g. Hall *et al.*, 2002; André,
45 2003; Thorn, 2004). André (1999) argued that understanding of periglacial environments has
46 been hidden in a ‘smokescreen’ of theories dominated by climate-driven geomorphic
47 processes involving frost, snow and ice, which were disconnected from the complex
48 processes that operate in periglacial domains. The application of paraglaciation theory in
49 geomorphological studies has emphasised the need for a deeper appreciation of the role of
50 non-glacial processes in present-day polar and high mountain environments (Ballantyne, 2002;
51 Mercier, 2008; André, 2009; Slaymaker, 2011). Berthling and Etzelmüller (2011) introduced
52 the concept of cryo-conditioning to unify interactions between cryotic surface and subsurface
53 thermal regimes and geomorphic processes in determining cold region landscape evolution.
54 An aspect that remains unexplored is the impact of periglacial and paraglacial processes on
55 the evolution of Arctic coastal zones (Figure 1) and in particular on rocky coastlines (Overduin
56 *et al.*, 2014). It is noteworthy that over three decades ago the lack of a consensus on the
57 efficiency of coastal processes in high latitudes was identified by Trenhaile (1983) and still
58 remains.

59 In the Arctic, sea ice extent and thickness has been declining by more than 10 % per decade
60 since satellite observations began in 1979 (NASA Earth Observatory). This decrease is
61 lengthening the period in which Arctic coastlines are vulnerable to storms and thermal
62 erosion, potentially increasing rates of coastal erosion (Lantuit *et al.*, 2012). In several parts
63 of the Arctic, accelerated glacier retreat has led to the exposure of new fragile coastal
64 systems, where evolution depends on permafrost-related processes and fluxes of sediments
65 from paraglacially transformed landforms. All these changes are expected to impact coastal
66 morphology, causing increased rates of erosion, extensively modifying near shore sediment

67 and organic carbon mobilization and transport, and potentially pushing coastal systems across
68 critical geomorphological and ecological thresholds (e.g. Fritz et al., 2017).

69 Up to 35% of Arctic coastlines are rock-dominated and large parts of community and
70 scientific infrastructure are located along rocky coasts (Forbes *et al.* 2011), but few studies
71 have focused specifically on this environment (see Hansom *et al.* 2014 for a comprehensive
72 review). Previous and classic works on Arctic rock coasts systems emphasized the role of
73 icefoot (e.g. Jahn, 1961; Dionne, 1973; Nielsen, 1979), snow cover (e.g. Ødegård *et al.*, 1995),
74 sea ice and frost weathering (e.g. Trenhaile, 1983; Dionne and Brodeur, 1988; Fournier and
75 Allard, 1992; Guilcher *et al.*, 1994; Lundberg and Lauritzen, 2002; Wagensteen *et al.*, 2007)
76 as key controls of shore platform and cliff face geomorphology in polar settings. More recent
77 studies carried out in Svalbard have focused on detailing the characteristics of rock coast
78 weathering using Schmidt hammer rock tests (Strzelecki, 2011; Strzelecki, 2016). Swirad *et al.*
79 (2017) analysed rock control on the geometry of northern Hornsund coastline. An important
80 progress in understanding of Svalbard coastal systems was recently made by Kasprzak *et al.*
81 (2016), who used electrical resistivity tomography (ERT) to demonstrate strong influence of
82 the sea on the coastal permafrost base. Previously, this issue has been often overlooked in
83 Arctic coastal studies or hidden under schemas (e.g. Lachenbruch, 1968; Gold and
84 Lachenbruch, 1973), which cannot be universally applied for diverse Arctic coastal systems.

85 The overarching aim of this study is to characterise the mechanisms controlling
86 present-day development of rocky coastal zone in High Arctic fjord environment with
87 particular focus on the spatial changes in distribution of coastal permafrost and the degree of
88 rock surface weathering along landforms evolving in various lithologies. In this paper we
89 summarise the results of our recent investigations into cryo-conditioned rock coast systems
90 in Svalbard. We have applied a combination of geomorphological and geophysical methods to
91 identify and characterise the effects of periglacial processes operating on rocky cliffs and shore

92 platforms and propose a new conceptual model of the functioning of High Arctic rock coast
93 systems.

94
95 **2. Regional setting**
96

97 The research was undertaken along the rocky coast of Wilczekodden (76.9964°N;
98 15.5458°E), a small (approx. 500 × 150 m) cape located in Hornsund between the
99 Rettkvalbogen and Isbjørnhamna embayments (Figure 2).

100 Due to the warm and humid air masses transported by cyclones and warm West Spitsbergen
101 Current, the climatic conditions in Hornsund (Osuch and Wawrzyniak, 2017). The
102 meteorological data published online at www.glacio-topoclim.org/reports, show that the
103 mean annual air temperature (MAAT) during the period from 1979 to 2014 was -4.0°C . The
104 warmest month was July, with an average temperature of 4.5°C , the coldest was March, with
105 an average temperature of -10.4°C . The mean annual precipitation total was 453 mm, but
106 varied significantly from 230.2 mm in 1987 to 635.9 mm in 1996 (Marsz and Styszyńska, 2013).
107 Snow cover thickness reached ca. 0.7 m on the ice-bounded fjord and 1.5 m in the valleys,
108 and wind-blown snow accumulated to depths of more than 3 m at the foot of the cliffs.

109 The configuration of an adjacent fjord and bordering mountain ranges produce strong
110 topographic control on local wind patterns. Mountains limit northern and southern air masses,
111 which were responsible for only 5.1 % of total detected winds for 1979–2006. Dominant wind
112 directions were recorded from: east (44.1 %), north-east (17.7 %) and west (12.1 %). Mean
113 wind speed in the area is 5.6 m s^{-1} (Kępski et al., 2013). The length (ca. 30 km) and width (14.5
114 km at the mouth) of open water in the fjord to the west expose the Wilczekodden to long
115 oceanic waves, whilst dominant eastern winds create short, low wind waves that operate
116 within the inner fjord shore. Glacier calving also creates low-frequency waves that modifies
117 the geomorphology of local gravel-dominated barriers (Zagórski et al., 2015).

118 The main geomorphological processes operating on the local strandflat and valley
119 systems reflect both periglacial weathering of relict coastal and glacial landforms and
120 paraglacial remodelling dominated by slope (e.g. Skolasińska et al., 2016; Hartvich et al., 2017),
121 fluvial (e.g. Owczarek et al., 2014; Wawrzyniak et al., 2017), coastal (e.g. Zagórski et al., 2015;
122 Swirad et al., 2017) and permafrost-related processes (e.g. Kasprzak, 2015; Kasprzak et al.,
123 2016). During the last century, all glaciers in the surrounding area have experienced rapid
124 retreat which accelerated between 2001 and 2010 when it reached $\sim 3 \text{ km}^2 \text{ a}^{-1}$ (Błaszczuk et
125 al., 2013). Until the early 1990's the active layer thickness varied around average, 1 - 1.15 m
126 (Baranowski, 1968; Jahn, 1982; Migąła, 1994), and due to the climate warming ground thawing
127 depth has recently exceeded 2 m (Dolnicki et al., 2013). However, the active layer
128 development in Hornsund is strongly dependent on ground lithology and land cover, in
129 addition to summer thermal conditions (Migąła et al., 2014). For instance, the thickness of the
130 active layer developed in marine gravels and sands was recorded at 2.3 m in late 1980's (Chmal
131 et al., 1988). Frozen ground conditions are extensive and vary from thick and continuous
132 permafrost in mountainous areas to thin (0–10 m), recently developed in deglaciated valleys
133 and along the coast (e.g. Kasprzak et al., 2016).

134 The north-western part of Hornsund is formed from Precambrian rocks, which are a
135 part of the lower and middle Hecla Hoek succession, overlain by Cambrian and Ordovician
136 rock layers (Smulikowski, 1968). Marbles and schists are present at Wilczekodden (Czerny et
137 al., 1992a). Karczewski et al. (1981b) defined 15 levels of raised marine terraces in the
138 Hornsund area covering the extensive strandflat of SW Spitsbergen. Glacial and periglacial
139 landforms (e.g. outwash plains, moraines, roches moutonnées and pingos) cover a significant
140 part of the north-western Hornsund strandflat.

141 Wilczekodden is a rocky cape covered by a series of uplifted marine terraces, forming
142 distinct levels up to 1-2 m high. The fairly evenly distributed marine terraces are studded with

143 strongly-weathered rocky outcrops (up to 2 m high) associated with relict skerries. Rocky
144 cliffs are present all around the cape, reaching 6 m high along the western marble coast (Figure
145 2 F) and up to 3 m high along the eastern shale coast (Figure 2 D). The tip of the cape is
146 covered by a steep staircase of raised gravel-dominated beaches, a remnant of still active
147 glacio-isostatic uplift in the area. Accumulations of marine pebbles are also found in several
148 shallow hollows spread across the cape. They are periodically filled with snowmelt waters.
149 Most uplifted marine sediments are sorted by periglacial processes and forms various types
150 of patterned grounds (circles, stripes). The rest of the cape surface is overlaid by coarse
151 weathered debris often vegetated by dry tundra.

152

153 **3. Materials and methods**

154 *3.1 Mapping coastal permafrost using geophysical methods*

155 Electrical resistivity tomography (ERT) allows identification of ground thermal conditions (e.g.
156 Hauck, 2002; Hauck and Krautblatter, 2007; Lewkowicz et al., 2011). The method is based on
157 the application of an electric current into the ground and measurement of the intensity of
158 electrical resistivity. During ERT the electric current (I) is transmitted to the ground through
159 two electrodes and the potential difference (V) is measured by a second pair of electrodes.
160 Since the bedrock/ground is not a homogeneous body the measured resistivity, which
161 expresses the ratio of voltage to current (taking into account a coefficient (k), dependent
162 upon the configuration of the electrodes), is treated as the apparent resistivity. By traversing
163 ERT measurements along a profile and increasing the spacing between the electrodes multiple
164 measurement points can be collected and arranged in separate horizons.

165 The geophysical surveys utilised the ARES ERT system (GF Instruments, Brno, Czech
166 Republic). The surveys were conducted between 4th and 7th of August 2015 and consisted of
167 four profile lines (Figure 3).

168 Along the Wilczekodden main profile (P1, Figure 3; 555 m long) and three shorter transverse
169 profiles (Figure 3: P2-4; 155-315 m long). Measurements along each profile have been
170 conducted at 5 m spacing between electrodes. A Werner-Schlumberger electrode array was
171 used to obtain high quality vertical resolution and depth penetration (Loke, 2000; Milsom,
172 2003; Reynolds, 2011). The results of apparent resistivity have been subjected to standard
173 geophysical interpretation (inversion) using RES2DINV software (Geotomo, Malaysia). The
174 default smoothness-constrained inversion formula (least squares inversion, initial Damping
175 factor = 0.160, minimum Damping factor = 0.015) has also been applied to the data. As a
176 result, the inversion models have been visualized for 3 iterations using a uniform colour scale.
177

178 *3.2 Observations of rock weathering and down-wearing processes*

179 *3.2.1 Schmidt hammer rock tests*

180 An electronic N-Type Silver Schmidt Hammer manufactured by Proceq was used in
181 this study. The Schmidt hammer measures the rebound of a spring-loaded mass as it impacts
182 on a rock surface providing an arbitrary measure of rock resistance on a scale with a value
183 range 10-100. Six locations were selected along the Wilczekodden coastline (Figure 4) to
184 encompass both main rock types (schist and marble) and the diverse morphologies (note the
185 differences between the east and west sides of the cape, Figure 2).

186 At each of the six locations the SHRT readings were taken at five elevations: in the
187 intertidal zone, at the high-water level, cliff toe, cliff face and cliff top (Figure 5). Each test
188 comprised of 25 measurements made at points randomly selected from a *ca.* 0.10 × 0.10 m
189 area. The statistical study by Niedzielski et al. (2009) suggested that this number of readings
190 provides an appropriate accuracy of SHRT in the majority of lithologies.

191 Measurements were conducted on sunny and warm days when the rock surfaces
192 located within the intertidal zone had dried out. The tests were conducted at least 0.05 m

193 from cracks and rock edges and on lichen-free areas following the methodology of Day and
194 Goudie (1977) and Selby (1980).

195

196 3.2.2 *Traversing Micro-Erosion Meter*

197 Traversing Micro-Erosion Meters (TMEMs) measure erosion caused by mechanical,
198 chemical and biological processes with a high precision positioning system based on oblique
199 coordinates. Over the last 30 years TMEMs have been used successfully to study rock surface
200 down-wearing rates in coastal environments (see Stephenson and Finlayson (2009) for a
201 review). Readings are taken by placing the triangular base of the instrument on three bolts
202 that are permanently fastened to a rock surface. The exact re-positioning of the instrument
203 on bolts is possible since each leg has different ends (flat, trench and pit), which also eliminates
204 instrument horizontal movement. The readings are carried out using an engineering dial gauge
205 that is independent of the triangular base and is moved to a number of set positions across
206 the area between three bolts.

207 TMEM used in this study was designed and manufactured by Albatros Marine
208 Technologies (Palma de Mallorca, Spain). We installed six TMEM stations along two profile
209 lines: TM1-TM3 in marbles and TM4-TM6 in schists (Figure 4). At least 10 readings were
210 collected from each TMEM station, generating reasonable estimates of rates of surface change
211 (Trenhaile and Lakhan, 2011). In each profile, the TMEM stations were installed at three
212 locations: in the intertidal zone, at the cliff toe and cliff top. Damage by sea ice action on the
213 bolts installed in schists (TM4-TM6) prevented sufficient readings of surface change.
214 Therefore, the rates of change observed between 02.08.2015 and 21.07.2016 have been
215 established only from stations TM1-TM3 installed in marbles.

216

217 **4. Results and Discussion**

218

219 4.1 Geophysical surveys

220 The ERT surveys have revealed the main geoelectrical features of the Wilczekodden
221 cape (Figure 6). The depth of geoelectrical imaging was dependent on the number of
222 electrodes used and the length of the profiles, which ranged from 26 m for P2 with 9
223 measurement horizons to 82 m for the P1 with 17 measurement horizons. In each case the
224 highest (upper) horizon of measurement points was located at 2.5 m below the ground
225 surface.

226 The results indicate large contrasts in the geoelectrical characteristics of the ground
227 (electrical resistivity). In the longitudinal profile along the cape (P1, Figure 6), a zone of high
228 resistivity ($\rho > 10 \text{ k}\Omega\cdot\text{m}$) decreases seaward and the influence of mean sea-level on reducing
229 resistivity values is clearly evident at the cliff edge at the cape's southern point. In all cross-
230 section profiles (P2-P4, Figure 6) the highest resistivity zones ($\rho > 10 \text{ k}\Omega\cdot\text{m}$) were situated up
231 to 10 m below the surface.

232 In the interior of the cape, distant from the sea, the thickness of the layer characterized
233 by high resistivity increases to 30-40 meters below the ground surface (P3 and P4 in Figure
234 6). Additionally, P3 revealed an isolated zone of low resistivity $\rho < 1 \text{ k}\Omega\cdot\text{m}$ detected near the
235 ground surface (Figure 6). The thin weathering surface and relatively simple geology of the
236 Wilczekodden (schists in the east and marbles in the west) aids interpretation of the thermal
237 state of the ground. High values of resistivity are associated with the presence of permafrost.
238 Various values for resistivity of frozen ground are have been provided by previous studies,
239 dependant on many factors (e.g. moisture content, physical characteristics of the rock), but it
240 is generally assumed that bodies with resistivity $\rho > 1 \text{ k}\Omega\cdot\text{m}$ generally indicate ice content (e.g.
241 McGinnis et al., 1973; Larin et al., 1978; Arcone and Delaney, 1988; Rein et al., 2004; Halley
242 et al., 2007), although this value can be of a larger magnitude (MacKay, 1969) and such is taken
243 into account in our interpretation ($\rho > 10 \text{ k}\Omega\cdot\text{m}$).

244 In Wilczekodden the development of permafrost extends from the cape surface to ca.
245 40 m below the ground. The permafrost forms a wedge orientated towards the shoreline
246 where the thickness of the permafrost layer is reduced and restricted to elevations above
247 present sea-level. The sea-contact control, related to the thermal influences of water
248 temperature and salinity, has parallels with the findings at other nearby embayments: Steinvika,
249 Hyttevika and Veslebogen by Kasprzak et al. (2016).

250 The anomaly detected in P3 results from a depression covered with marine pebbles
251 and episodically filled by water, that is likely to disturb the thermal state of the ground by
252 thermoerosion (Figure 6). The measurement resolution, with an upper measurement horizon
253 located at 2.5 m below the surface, did not allow detection of active layer extents.

254 The ERT measurements have indicated the strong influence of the sea on
255 ground/bedrock thermal characteristics in the coastal zone. In summer, both surface water
256 and groundwater are subjected to rising temperatures and salinity due to fjord water ingress
257 (Węśławski 2011). The interpretation of ERT inversion models demonstrates that in the
258 Hornsund region, proximity to coastal waters restricts the development of permafrost.
259 Despite the dependence on assumptions regarding the lithological, structural and textural
260 properties of the ground, similar interpretations have been made in other periglacial
261 environments (e.g. Mackay, 1972; Seguin et al., 1988; Hauck, 2002; Ishikawa, 2004;
262 Krautblatter and Hauck, 2007; Kneisel et al., 2008; Hilbich et al., 2009; You et al., 2013; Kneisel
263 et al., 2014).

264

265 4.3. Rock strength and surface change observations

266 4.3.1 Schmidt hammer rock tests

267 Schmidt hammer rock tests showed that the rock strength varies considerably as a function
268 of rock type, location along the coast and vertical location at each site (Figure 7). In all cases

269 the highest and most consistent (lowest error) R-values (65-75) were recorded in the
270 intertidal zone, while the lowest and most variable R-values (30-52) occurred at the cliff top.
271 In general, the marble cliff sites (M1-M3, Figure 7) recorded higher strength (hardness
272 rebound) values, reducing less with elevation and exhibiting lower variability (<20 if cliff top
273 of M3 excluded). Rock hardness is much more diverse for the schist cliff sites (S1-S3), as the
274 R-values do not decrease consistently when moving up the cliff and the standard error remains
275 relatively high (up to 3.8). Site M3 has the most significant (of 45) reduction of hardness values
276 from the intertidal zone to the cliff top.

277 The two rock types of the Wilczekodden respond to weathering and erosive
278 processes differently. At the marble cliff sites, the rock strength and hardness consistency
279 decrease systematically landwards from the intertidal zone. In contrast, at the schist cliff sites
280 the R-value distribution is not consistent between cross-profiles. The discrepancy may be due
281 to differences in micro-structure of the two rock types, where marble is more massive and
282 schist is composed of thin layers with strong orientation control (Swirad et al., 2017). In
283 general, rock strength is the lowest on the cliff top where wave action is absent and
284 weathering due to nivation, freeze-thaw and wet-dry cycles is intense.

285 The strength of the rock surface depends on the intact rock mass strength (directly
286 linked with rock type and structure) and deterioration due to weathering (Selby, 1980). Chelli
287 et al., (2010) noticed that in coastal settings the strength depends on both the type of rock
288 and mechanical weathering (wetting/drying cycle).

289 Along the Wilczekodden the level of weathering due to wetting and drying varies
290 considerably in relation to tidal inundation and patterns of wave action. In periglacial
291 environments further process control is exerted by the presence and movement of sea ice,
292 the formation of an icefoot, partial snow cover and freeze-thaw weathering (e.g. Trenhaile,
293 1997; Hansom et al., 2014; Strzelecki, 2016).

294 In the intertidal zone the rock surface is eroded by wave and sea ice action, removing the
295 weathering surface (Blanco-Chao et al., 2007) and leading to higher and more repeatable
296 (consistent) Schmidt hammer reading in this zone (Williams and Robinson, 1983; Goudie,
297 2006). The increasing weathering influence with elevation above sea-level is similar to patterns
298 observed on sandstone and anhydrite cliffs in Billefjorden, central Spitsbergen (Strzelecki,
299 2016).

300

301 *4.3.2 Traversing micro-erosion meter measurements*

302 The average surface change at each station has been derived by calculating the total
303 erosion/swelling present at each measurement point and dividing by the number of points.
304 Over the study period, the stations experienced surface change at different rates according
305 to their elevation. The down-wearing of the rock surface was observed only at station TM2
306 installed at the cliff toe (mean surface vertical erosion -1.2 mm). At the top of the cliff (TM1,
307 Figure 8) the surface remained unchanged, whereas surface swelling was observed at station
308 TM3 installed in the intertidal zone (mean surface elevation 0.2 mm).

309 Although limited to one profile, these observations demonstrate that micro-erosion
310 occurred only at coastal elevations subject to wave impacts and to the most frequent and
311 complete shifts in wetting and drying where wetting from tides, waves and spray are often
312 completely dried out before rewetting. The swelling observed on the surface of shore
313 platform is a relatively common process associated with crystallization of salt, algae growth,
314 heating and cooling as well as wetting and drying (Stephenson and Finlayson, 2009).

315 In High Arctic settings, such as Svalbard, the remaining question is the role of
316 stagnation and melting of sea-ice floes on the surface of shore platforms leading to significant
317 cooling of rock surfaces regardless of daytime heating. Values of rock surface swelling

318 observed in Wilczekodden were similar to those from other morphoclimatic sites (e.g.
319 Stephenson and Kirk 2001; Trenhaile, 2006).

320

321 *4.4 Implications for the conceptual model of a High Arctic rock coast system*

322 In order to develop a general model of cryo-conditioned rocky coast zones developing
323 in polar regions, a schematic summary of the dominant processes is presented in Figure 9.

324 Based on the observations of rocky shores forming along Wilczekodden and results of
325 previous rock coast studies in Svalbard (e.g. Jahn, 1961; Ødegård and Sollid, 1993; Ødegård
326 et al., 1995; Migoń, 1997; Wangensteen et al., 2007; Strzelecki, 2011; Kasprzak et al., 2016;
327 Strzelecki 2016; Swirad et al., 2017), the rocky coast system has been divided into seven
328 geomorphic zones (Table 1).

329 The evolution of High Arctic rocky coasts is associated with seasonal variability in sea
330 ice action, frost weathering, permafrost-dependent rock saturation and snow insulation
331 (Trenhaile and Mercan, 1984; Dawson et al., 1987). Strzelecki (2016) highlighted the role of
332 debris cover and bioagents (driftwood, seaweeds, birds) in shaping cold region rocky cliff and
333 platform morphology.

334 High Arctic coastal regions are also characterised by microtides and reduced wave
335 action due to sea ice cover. Therefore, it is possible to isolate the relative importance of rock
336 resistance and wave-, tide- and frost-induced processes on coastal morphology.

337 The two existing models of periglacial shore platform evolution proposed by Hansom
338 (1983) for South Shetland Islands, Antarctica and Fournier and Allard (1992) for Ungava Bay,
339 Arctic envisage rapid adjustment of coastlines, partially inherited from former sea high stands
340 to the present morphoclimatic environment.

341 A somewhat different situation may exist along High Arctic coastlines, which have
342 been exposed to coastal processes for the first time during the Holocene. In these settings,

343 coastal evolution is strongly influenced by post-glacial rock debuttressing, the rate of land
344 uplift and relative sea-level changes. Many High Arctic archipelagos such as Svalbard, the
345 Canadian Arctic Archipelago, Franz Josef Land, Novaya Zemlya have experienced rapid coastal
346 emergence or submergence related glacio-isostatic adjustment to deglaciation and associated
347 with relative sea-level (RSL) changes (e.g. Forman et al., 2004; Long et al., 2012). Therefore,
348 High Arctic rocky coastlines provide an excellent test area for various hypotheses in shore
349 platform development in periglacial conditions as yet described mainly on lacustrine examples
350 from Scotland (Sissons, 1978; Dawson, 1980), Norway (Matthews et.al, 1986; Dawson et al.,
351 1987; Shakesby and Matthews, 1987; Aarseth and Fosgen, 2004) and Canada (Trenhaile, 2004).
352 The well-dated chronology of RSL change based on widespread uplifted beaches provides a
353 useful basis for exploration of the time-dependence of cliff and platform evolution, as well as
354 the operation of geomorphic processes. For instance, the development of coastal karst dolina
355 relief in Vardeborgsletta, characteristic for carbonate and evaporite outcrops in central and
356 eastern Spitsbergen, has been strongly linked with sea-level change (Salvigsen and Elgersma,
357 1985). Karstic processes in rocky coasts are likely to have been initiated during Holocene sea-
358 level highstands, when frozen rocks thawed and subsequently emerged due to rapid
359 glacioisostatic uplift. More recently a novel study by Hanken et al. (2012) indicated that the
360 presence of polychaete borings in subaerially exposed bedrock surfaces can be used to
361 evaluate postglacial emergence on Svalbard in the absence of well-preserved uplifted beach
362 sediments or isolation basins.

363

364 **5. Conclusions**

365 For the first time in the High Arctic setting the rock coast system has been investigated using
366 the combination of geomorphological (SHRT, TMEM) and geophysical (ERT) methods. Based
367 on the observations we have drawn the following conclusions:

368
369
370
371
372
373
374
375
376
377
378
379
380
381
382
383
384
385
386
387
388
389
390
391
392

1. The development of permafrost along Wilczekodden rocky coast is controlled by the thermal influence of sea water. Coastal permafrost evolves in the form of a wedge directed towards the shoreline.
2. Rock surface strength across shore platforms and cliffs depends on the efficiency of processes removing weathered and eroded material. In both tested lithologies (marbles and schists), the lowest rock strengths were observed along the top of the cliffs, subject primarily to periglacial weathering, whereas erosional processes operating across shore platforms and cliff bases lead to exposure of fresh and resistant rock surfaces.
3. For the first time in Hornsund, we have analysed the changes of rock surfaces using a traversing micro-erosion meter. Significant differences exist in the behaviour of rock surfaces located at the cliff top, cliff toe, and in the intertidal zone. Surface down-wearing occurred only at the base of the cliff exposed to frequent wetting and drying, storm wave impact and changes of thickness, duration and degradation of snowpatches and icefoot complexes.
4. Future research in High Arctic settings should include the role of processes associated with the frost and ice action. In addition, it is important that future studies consider: the spatial distribution of permafrost; the significance of diurnal and annual freeze-thaw cycles modified by wetting and drying; the influence of reduced icefoot size on the rock cliff and platform evolution; the climate-driven incorporation of debris from cliff abrasion into sea ice; type of bioagents operating on coastal rock surface, and finally, the impact of recently delivered paraglacial sediments on erosion or protection of rocky shorelines.

393

394 **Acknowledgements:**

395 This is a contribution to the National Science Centre project UMO2013/11/B/ST10/00283: ‘
396 POROCO – Mechanisms controlling the evolution and geomorphology of rock coasts in polar
397 climates’. Matt Strzelecki is supported by NCN Postdoctoral Fellowship FUGA and the
398 Ministry of Science and Higher Education Outstanding Young Scientist Scholarship. The author
399 thanks the participants of 11th International Conference on Permafrost their constructive
400 comments on the results presented in this study. We thank reviewers Professor Alan
401 Trenhaile and Filip Hrbacek, and the Editor for their very thoughtful and constructive
402 comments, which significantly improved the manuscript. This research is a contribution to the
403 IAG Sediment Budgets in Cold Environments Working Group.

404

405 **References:**

- 406 Aarseth, I., Fosgen H., 2004. A Holocene lacustrine rock platform around Storavatnet,
407 Osterøy, western Norway. *Holocene* 14: 589-596.
- 408 André, M-F., 1999. La livrée périglaciaire des paysages polaires: l'arbre qui cache la forêt? The
409 periglacial scenery of polar areas: a smoke-screen? *Géomorphologie: relief, processus,*
410 *environnement* 5: 231 – 251.
- 411 André, M-F., 2003. Do periglacial landscapes evolve under periglacial conditions?
412 *Geomorphology* 52: 149-164.
- 413 André, M-F., 2009. From climatic to global change geomorphology: contemporary shifts in
414 periglacial geomorphology. In Knight J., and Harrison S., (Eds.) *Periglacial and Paraglacial*
415 *Processes and Environments*. Geological Society, London Special Publications 320: 5-28.
- 416 Arcone, S.A., Delaney, A.J., 1988. Borehole investigations of the electrical properties of frozen
417 silt. In: Senneset, K. (Ed.), *Permafrost. Fifth International Conference. August 2–5,*
418 *Proceedings Volume 2, Tapir Pub., Trondheim, Norway, pp. 910–915.*
- 419 Ballantyne, C., 2002. Paraglacial geomorphology. *Quaternary Science Reviews* 21: 1935–2017.
- 420 Baranowski, S. 1968. Thermic conditions of the periglacial tundra in SW Spitsbergen. *Acta*
421 *Universitatis Wratislaviensis* 68: 74 pp.
- 422 Berthling, I., Etzelmüller B., 2011. The concept of cryo-conditioning in landscape evolution.
423 *Quaternary Research* 75: 378-384.
- 424 Blanco-Chao, R., Pérez-Alberti, A., Trenhaile, A.S., Costa-Casais, M., Valcárcel-Díaz, M., 2007.
425 Shore platform abrasion in a para-periglacial environment, Galicia, northwestern Spain.
426 *Geomorphology* 83: 136–151.
- 427 Błaszczuk, M., Jania, J., Kolondra, L., 2013. Fluctuations of tidewater glaciers in Hornsund Fjord
428 (Southern Svalbard) since the beginning of the 20th century. *Polish Polar Research* 34: 327-
429 352.

430 Byrne, M-L., Dionne, J-C., 2002. Typical Aspects of Cold regions Shorelines. In: Hewitt K.,
431 Byrne M-L., English M., Young G., (Eds.), Landscapes in Transition. Landform Assemblages
432 and Transformations in Cold Regions. Kluwer Academic Publishers, Dordrecht: 141- 158.

433 Chelli, A., Pappalardo, M., Llopis, I.A., Federici, P. B., 2010. The relative influence of lithology
434 and weathering in shaping shore platforms along the coastline of the Gulf of La Spezia (NW
435 Italy) as revealed by rock strength. *Geomorphology* 118: 93-104.

436 Chmal, H., Klementowski, J., Mięgała, K., 1988. Thermal currents of active layer in Hornsund
437 area. In: Senneset, K. (Ed.), Permafrost. Fifth International Conference. August 2–5,
438 Proceedings Volume I, Tapir Pub., Trondheim, Norway, pp. 44–49.

439 Czerny, J., Kieres, A., Manecki, M., Rajchel, J., 1992. Geological Map of the SW Part of Wedel
440 Jarlsberg Land Spitsbergen, 1:25 000. Institute of Geology and Mineral Deposits, Univ. of
441 Mining and Metallurgy, Cracow.

442 Davies, J. L., 1980. Geographical Variation in Coastal Development. London: Longman Group
443 Ltd., 212p.

444 Dawson, A. G., Matthews, J. A., Shakesby, R. A., 1987. Rock platform erosion on periglacial
445 shores: a modern analogue for Pleistocene rock platforms in Britain. In Boardman, J. (ed.):
446 Periglacial processes and landforms in Britain and Ireland. Cambridge University Press,
447 Cambridge 173--182.

448 Day, M.J., and Goudie, A.S., 1977. Field assessment of rock hardness using the Schmidt test
449 hammer. *British Geomorphology Research Group Technical Bulletin* 18: 19–29.

450 Dickson, M.E., Kennedy, D.M., Woodroffe, C.D., 2004. The influence of rock resistance on
451 coastal morphology around Lord Howe Island, Southwest Pacific. *Earth Surface Processes*
452 and Landforms 29: 629–643.

453 Dionne, J.-C., 1973. La motion de pied de glace (Ice-foot), en particulier dans l'estuaire du
454 Saint-Laurent, *Cahiers Géographie Québec* 17: 221–250.

455 Dionne, J.-C., Brodeur, D., 1988. Frost weathering and ice action in shore platform
456 development, with particular reference to Quebec, Canada. *Zeitschrift für*
457 *Geomorphologie Supplement band 71*: 117-30.

458 Dolnicki, P., Grabiec, M., Puczko, D., Gawor, Ł., Budzik, T., Klementowski, J., 2013. Variability
459 of temperature and thickness of permafrost active layer at coastal sites of Svalbard. *Polish*
460 *Polar Research 34*: 353–374.

461 Forbes, D.L. (editor), 2011. *State of the Arctic Coast 2010 – Scientific Review and Outlook.*
462 *International Arctic Science Committee, Land-Ocean Interactions in the Coastal Zone,*
463 *Arctic Monitoring and Assessment Programme, International Permafrost Association.*
464 *Helmholtz-Zentrum, Geesthacht, Germany: 178; <http://arcticcoasts.org>*

465 Forman, S., Lubinski, D., Ingolfsson, O., Zeeberg, J., Snyder, J., Siegert, M., Matishov, G., 2004.
466 A review of postglacial emergence on Svalbard, Franz Josef Land and Novaya Zemlya,
467 northern Eurasia. *Quaternary Science Reviews 23*: 1391–1434.

468 Fournier, A., Allard, M., 1992. Periglacial shoreline erosion of rocky coast: George River
469 Estuary, Northern Quebec. *Journal of Coastal Research 8*: 926-942.

470 Fritz, M., Vonk, J.E., Lantuit, H., 2017. Collapsing Arctic coastlines. *Nature Climate Change 7,*
471 *6-7. <http://dx.doi.org/10.1038/nclimate3188>.*

472 Gold, L.W., Lachenbruch, A.H., 1973. Thermal conditions in permafrost – a review of North
473 American literature. In: *Permafrost Second International Conference, 13–28 July 1973,*
474 *Yakutsk, U.S.R.R., North American Contribution, Arlis, National Academy of Sciences,*
475 *Washington, pp. 3–25.*

476 Goudie, A., 2006. The Schmidt Hammer in geomorphological research. *Progress in Physical*
477 *Geography 30*: 703–718.

478 Guilcher, A., Bodere, J.-C., Coude, A., Hansom, J. D., Moign, A. and Peullvast, J.-P. (1994) The
479 Strandflat problem in five high latitude countries. In: Evans, D. J.A. (ed.) Cold Climate
480 Landforms. Wiley: Chichester, pp. 351-393.

481 Hall, K., Thorn, C., Matsuoka, N., Prick, A., 2002. Weathering in cold regions.: Some thoughts
482 and perspectives. *Progress in Physical Geography* 4: 576-602.

483 Halley, K., Bentley, L.R., Gharibi, M., Nightingale, M., 2007. Low temperature dependence of
484 electrical resistivity: Implications for near surface geophysical monitoring. *Geophysical*
485 *Research Letters* 34, L18402, doi:10.1029/2007GL031124

486 Hanken N-M., Uchman, A., Jakobsen , S.L., 2012. Late Pleistocene-early Holocene polychaete
487 borings in NE Spitsbergen and their palaeoecological and climatic implications: an example
488 from the Basissletta area. *Boreas* 41: 42-55.

489 Hansom, J.D., 1983. Shore-platform development in the South Shetland Islands, Antarctica.
490 *Marine Geology* 53: 211-229.

491 Hansom, J.D., Forbes, D.L., Etienne, S., 2014. The rock coasts of polar and sub-polar regions.
492 In Kennedy D. M., Stephenson W. J. & Naylor L. A. (Eds) 2014. *Rock Coast*
493 *Geomorphology: A Global Synthesis*. Geological Society, London, *Memoirs*, 40: 263–281.

494 Hartvich, F., Blahut, J., Stemberk, J., 2017. Rock avalanche and rock glacier: A compound
495 landform study from Hornsund, Svalbard. *Geomorphology* 276: 244-256.

496 Hauck, C. 2002. Frozen ground monitoring using DC resistivity tomography. *Geophysical*
497 *Research Letters* 29(21): 2016, doi:10.1029/2002GL014995

498 Hilbich, C., Marescot, L., Hauck, C., Loke, M.H., Mäusbacher, R., 2009. Applicability of
499 Electrical Resistivity Tomography Monitoring to Coarse Blocky and Ice-rich Permafrost
500 Landforms. *Permafrost and Periglacial Processes* 20: 269–284.

501 Ishikawa, M., 2004, Application of DC resistivity imaging to frozen ground investigations.
502 *Journal of the Japanese Society of Snow and Ice* 66: 177–186.

503 Jahn, A., 1961. Quantitative analysis of some periglacial processes in Spitsbergen. *Zeszyty*
504 *Naukowe Uniwersytetu Wrocławskiego Seria B*, nr 5, Geophysics, Geography, Geology II:
505 3-54.

506 Jahn, A. 1982. Soil thawing and active layer of permafrost in Spitsbergen. *Acta Universitatis*
507 *Wratislaviensis* 525, Spitsbergen Expeditions IV, pp. 57–75.

508 Kasprzak, M., 2015. High-resolution electrical resistivity tomography applied to patterned
509 ground, Wedel Jarlsberg Land, south-west Spitsbergen. *Polar Research* 34(25678): 1-13.

510 Kasprzak, M., Strzelecki, M.C., Traczyk, A., Kondracka, M., Lim, M., Migąła, K., 2016. On the
511 potential for a bottom active layer below coastal permafrost: the impact of seawater on
512 permafrost degradation imaged by electrical resistivity tomography (Hornsund, SW
513 Spitsbergen). *Geomorphology*, <http://dx.doi.org/10.1016/j.geomorph.2016.06.01>

514 Kępski, D., Górski, Z., Benedyk, M., Szumny, M., Wawrzyniak, T., 2013. Meteorological
515 bulletin. Spitsbergen-Hornsund. Summary of the year 2-13. Polish Polar Station, Institute
516 of Geophysics, Polish Academy of Sciences.

517 Kneisel, C., Hauck, C., Fortier, R., Moorman, B., 2008. Advances in geophysical methods for
518 permafrost investigations. *Permafrost and Periglacial Processes* 19: 157–178.

519 Kneisel C., Emmert, A., Kästl, J., 2014. Application of 3D electrical resistivity imaging for
520 mapping frozen ground conditions exemplified by three case studies. *Geomorphology* 210:
521 71–82.

522 Krautblatter M. & Hauck C. 2007. Electrical resistivity tomography monitoring of permafrost
523 in solid rock walls. *Journal of Geophysical Research: Earth Surface* 112, F2, 2156–2202.

524 Lachenbruch, A.H. 1968. Permafrost. In: Fairbridge, R.W. (Ed.), *The encyclopedia of*
525 *geomorphology*. New York, Reinhold Pub. Corp., pp. 833–839.

526 Lantuit, H., Overduin, P.P., Couture, N., Wetterich, S., Are, F., Atkinson, D., Brown, J.,
527 Cherkashov, G., Drozdov, D., Forbes, D.L., Graves-Gaylord, A., Grigoriev, M., Hubberten,
528 H.W., Jordan, J., Jorgenson, T., Ødegård, R.S., Ogorodov, S., Pollard, W., Rachold, V.,

529 Sedenko, S., Solomon, S., Steenhuisen, F., Streletskaia, I., Vasiliev, A., 2012. The Arctic
530 Coastal Dynamics database. A new classification scheme and statistics on Arctic permafrost
531 coastlines. *Estuaries and Coasts* 35: 383-400.

532 Larin, S.M., Marov, G.P., Kholmyanskiy, M.A., Neizvestnov, Ya.V., 1978. Certain types of
533 geoelectric sections of the negative temperature belt in the arctic and subarctic connection
534 with exploration for subpermafrost. In: Sanger, F.J, Hyde, P.J. (Eds), *Permafrost Second
535 International Conference, 13–28 July 1973, Yakutsk, U.S.R.R., USSR Contribution, National
536 Academy of Sciences, Washington*, pp. 428–430.

537 Lewkowicz A.G., Etzelmüller B. & Smith S.L. 2011. Characteristics of discontinuous
538 permafrost based on ground temperature measurements and electrical resistivity
539 tomography, Southern Yukon, Canada. *Permafrost and Periglacial Processes* 22 320–342.

540 Loke, M.H. 2000. *Electrical imaging surveys for environmental and engineering studies. A
541 practical guide to 2-D and 3-D surveys*. Geotomo, Malaysia.

542 Long, A.J., Strzelecki, M.C., Lloyd, J.M., Bryant, C., 2012. Dating High Arctic Holocene relative
543 sea level changes using juvenile articulated marine shells in raised beaches. *Quaternary
544 Science Reviews* 48: 61-66.

545 Lundberg, J., Lauritzen, S-E., 2002. The search for an Arctic coastal karren model in Norway
546 and Spitzbergen. In: Hewitt K., Byrne M-L., English M. and Young G., (Eds.), *Landscapes in
547 Transition. Landform Assemblages and Transformations in Cold Regions*. Kluwer
548 Academic Publishers, Dordrecht: 185-203.

549 MacKay, D.K., 1969. Electrical resistivity measurements in frozen ground, Mackenzie Delta
550 area, Northwest Territories. *Association Internationale d’Hydrologie Scientifique, Actes
551 du Colloque de Bearest, Reprint Ser. 82, Department of Energy, Mines and Resources,
552 Inland Waters Branch, Ceuterick, Belgium*, pp. 363–375.

553 Mackay, J.R., 1972. Offshore permafrost and ground ice, Southern Beaufort Sea, Canada.
554 *Canadian Journal of Earth Sciences* 9(11), 1550–1561.

555 Marsz, A.A., Styszyńska, A. (Eds.). 2013. *Climate and Climate Change at Hornsund, Svalbard*.
556 Authors: J. Ferdynus, A.A. Marsz, A. Styszyńska - Gdynia Maritime University, E. Łupikasza,

557 T. Niedźwiedź - University of Silesia). The publishing house of Gdynia Maritime University,
558 Gdynia, 402 p.

559 Matthews, J., Dawson, A.G., Shakesby, R.A. 1986: Lake shoreline development, frost
560 weathering and rock platform erosion in an alpine periglacial environment, Jotunheimen,
561 southern Norway. *Boreas* 15: 33-50.

562 McGinnis, L.D., Nakao, K., Clark, C.C., 1973, Geophysical identification of frozen and
563 unfrozen ground, Antarctica. In: Permafrost Second International Conference, 13–28 July
564 1973, Yakutsk, U.S.R.R., North American Contribution, Arlis, National Academy of
565 Sciences, Washington, pp. 3–25.

566 Mercier, D., 2008. Paraglacial and paraperiglacial landsystems: concepts, temporal scales and
567 spatial distribution. *Géomorphologie: relief, processus, environnement* 4: 223-234.

568 Migąła, K., 1994. The characteristic features of the active layer of the permafrost in the climate
569 of Spitsbergen (in Polish with Eng. abstract). *Acta Universitatis Wratislaviensis* 1590 (Prace
570 Instytutu Geograficznego C, Meteorologia i Klimatologia) 1, 79–111.

571 Migąła, K., Wojtuń, B., Szymański, W., Muskała, P., 2014. Soil moisture and temperature
572 variation under different types of tundra vegetation during the growing season: A case
573 study from the Fuglebekken catchment, SW Spitsbergen. *Catena* 116, 10–18.

574 Migoń, P., 1997. Post-emergence modification of marine cliffs and associated shore platforms
575 in periglacial environment, SW Spitsbergen: implications for the efficacy of cryoplanation
576 processes. *Quaternary Newsletter* 81: 9–17.

577 Milsom, J., 2003. Resistivity methods. In: *Field Geophysics* 3rd Edition. Wiley, Chichester. 97–
578 116.

579 Niedzielski, T., Migoń, P., Placek, A., 2009. A minimum sample size required for Schmidt
580 Hammer measurements. *Earth Surface Processes and Landforms* 34: 1713–1725.

581 Nielsen, N., 1979. Ice-foot processes. Observations of erosion of the rocky coast, Disko,
582 West Greenland. *Zeitschrift für Geomorphologie* 23: 321-331.

583 Ødegård, R. S., Sollid J.L., 1993. Coastal cliff temperatures related to the potential for
584 cryogenic weathering processes, western Spitsbergen, Svalbard. *Polar Research* 12: 95-106.

585 Ødegård, R. S, Etzelmüller, B., Vatne G., Sollid J., 1995. Nearsurface spring temperatures in
586 an Arctic coastal cliff: possible implications of rock breakdown. In SLAYMAKER O. (Ed.):
587 Steepland geomorphology. Wiley, Chichester UK: 89–102. Osuch, M., Wawrzyniak, T.,
588 2017. Inter- and intra-annual changes in air temperature and precipitation in western
589 Spitsbergen. *International Journal of Climatology* 37: 3082–3097.

590 Overduin, P.P., Strzelecki, M.C., Grigoriev, M.N., Couture, N., Lantuit, H., St-Hilaire-Gravel
591 D., Günther, F., Wetterich, S., 2014. Coastal changes in the Arctic. In: Martini, I. P.,
592 Wanless, H. R. (eds.) *Sedimentary Coastal Zones from High to Low Latitudes: Similarities*
593 *and Differences*. Geological Society, London, Special Publications, 388: 103-129.

594 Owczarek, P., Nawrot, A., Migąła, K., Malik, I., Korabiewski, B., 2014. Flood-plain
595 responses to contemporary climate change in small High-Arctic basins (Svalbard,
596 Norway). *Boreas* 43: 384–402.

597 Rein, A., Hoffmann, R., Dietrich, P., 2004. Influence of natural time- dependent variations of
598 electrical conductivity on DC resistivity measurements. *Journal of Hydrology* 285: 215–
599 232.

600 Reynolds, J.M., 2011. *Electrical Resistivity Methods*. In: *An Introduction to Applied and*
601 *Environmental Geophysics*. 2nd Ed., Wiley, Chichester, pp. 289–372.

602 Salvigsen, O., Elgersma, A., 1985. Large-scale karst features and open taliks at Vardeborgsletta,
603 outer Isfjorden, Svalbard. *Polar Research* 3: 145—153.

604 Seguin, M.K., Gahe, E., Allard, M., Ben-Mikoud, K. 1988. Permafrost geophysical investigation
605 at the new airport site of Kangiqsualujjuaq, Northern Quebec, Canada. In: Senneset, K.

606 (Ed.), Permafrost. Fifth International Conference. August 2–5, Proceedings Volume 2, Tapir
607 Pub., Trondheim, Norway, pp. 980–987.

608 Selby, M.J., 1980. A rock mass strength classification for geomorphic purposes: with test from
609 Antarctica and New Zealand. *Zeitschrift für Geomorphologie* 24: 31–51.

610 Shakesby, R.A., Matthews, J.A., 1987. Frost weathering and rock platform erosion on
611 periglacial lake shorelines: a test of a hypothesis. *Norsk Geologisk Tidsskrift* 67: 197-203.

612 Sissons, J.B., 1978. The parallel roads of Glen Roy and adjacent glens, Scotland. *Boreas* 7: 229-
613 44.

614 Skolasińska K., Rachlewicz G., Szczuciński W., 2016. Micromorphology of modern tills in
615 southwestern Spitsbergen - Insights into depositional and post-depositional processes.
616 *Polish Polar Research* 37: 435-456.

617 Slaymaker, O., 2011. Criteria to distinguish between periglacial, proglacial and paraglacial
618 environments. *Quaestiones Geographicae* 30: 85–94.

619 Smulikowski, W. (1968): Some petrological and structural observations in the Hecla Hoek
620 succession between Werenskioldbreen and Torelbreen, Vestspitsbergen. *Studia*
621 *Geologica Polonica* 21: 97-161.

622 Stephenson, W.J., Kirk, R.M., 2001. Surface swelling of coastal bedrock on inter-tidal shore
623 platforms, Kaikoura Peninsula, South Island, New Zealand. *Geomorphology* 41: 5-21.

624 Stephenson, W.J., Finlayson, B.L., 2009. Measuring erosion with the micro-erosion meter–
625 contributions to understanding landform evolution. *Earth Science Reviews* 95:53–62.

626 Strzelecki, M.C., 2011. Schmidt hammer tests across recently deglaciated rocky coastal zone
627 – is there a ‘coastal amplification’ of rock weathering in polar climates? *Polish Polar*
628 *Research* 32: 239-252.

629 Strzelecki, M.C., 2016, The variability and controls of rock strength along rocky coasts of
630 central Spitsbergen, High Arctic. *Geomorphology*, doi: 10.1016/j.geomorph.2016.06.014

631 Swirad, Z.M., Migoń, P., and Strzelecki, M.C., 2017. Rock control on the geometry of coastal
632 embayments of north-western Hornsund, Svalbard, *Zeitschrift für Geomorphologie* 61(1):
633 11-28.

634 Thorn, C., 2004. Whither, or wither, periglacial weathering studies? *Polar Geography* 28: 4-
635 12.

636 Trenhaile, A.S., 1983. The development of shore platforms in high latitudes. In: D.E. Smith and
637 A.G. Dawson (eds.), *Shorelines and Isostasy*. Institute of British Geographers, Special
638 publication No. 16, London: 77-96.

639 Trenhaile, A.S., 1997. *Coastal Dynamics and Landforms*. Oxford University Press, Oxford, UK,
640 pp.366.

641 Trenhaile, A.S., 2002. Modeling the effect of weathering on the evolution and morphology of
642 shore platforms. *Journal of Coastal Research* 17: 398–406.

643 Trenhaile, A.S., 2004. Lacustrine shore platforms in southwestern Ontario, Canada. *Zeitschrift*
644 *für Geomorphologie* 48: 441-459.

645 Trenhaile, A.S., 2006. Tidal wetting and drying on shore platforms: An experimental study of
646 surface expansion and contraction. *Geomorphology* 76: 316-331.

647 Trenhaile, A.S., Mercan, D.W., 1984. Frost weathering and the saturation of coastal rocks.
648 *Earth Surface Processes and Landforms* 9: 321–331.

649 Trenhaile, A.S., Lakhan, V.C., 2011. Transverse micro-erosion meter measurements;
650 determining minimum sample size. *Geomorphology* 134: 431–439

651 Trenhaile, A.S., Perez Alberti, A., Martinez Cortizas, A., Costa-Casais, M., Blanco Chao, R.,
652 1999. Rock coast inheritance: an example from Galicia, Northwestern Spain. *Earth Surface*
653 *Processes and Landforms* 24: 1 – 17.

654 Viles, H., Goudie, A., Grab, S., Lalley, J., 2011. The use of the Schmidt Hammer and Equotip
655 for rock hardness assessment in geomorphology and heritage science: a comparative
656 analysis. *Earth Surface Processes and Landforms* 36: 320-333.

657 Wangensteen, B., Eiken, T., Ødegård, R.S., Sollid, J.L., 2007. Measuring coastal cliff retreat in
658 the Kongsfjorden area, Svalbard, using terrestrial photogrammetry. *Polar Research* 26: 14–
659 21.

660 Wawrzyniak, T., Osuch, M., Nawrot, A., Napiorkowski, J. 2017. Run-off modelling in an Arctic
661 unglaciated catchment (Fuglebekken, Spitsbergen). *Annals of Glaciology*, 1-11.
662 doi:10.1017/aog.2017.8

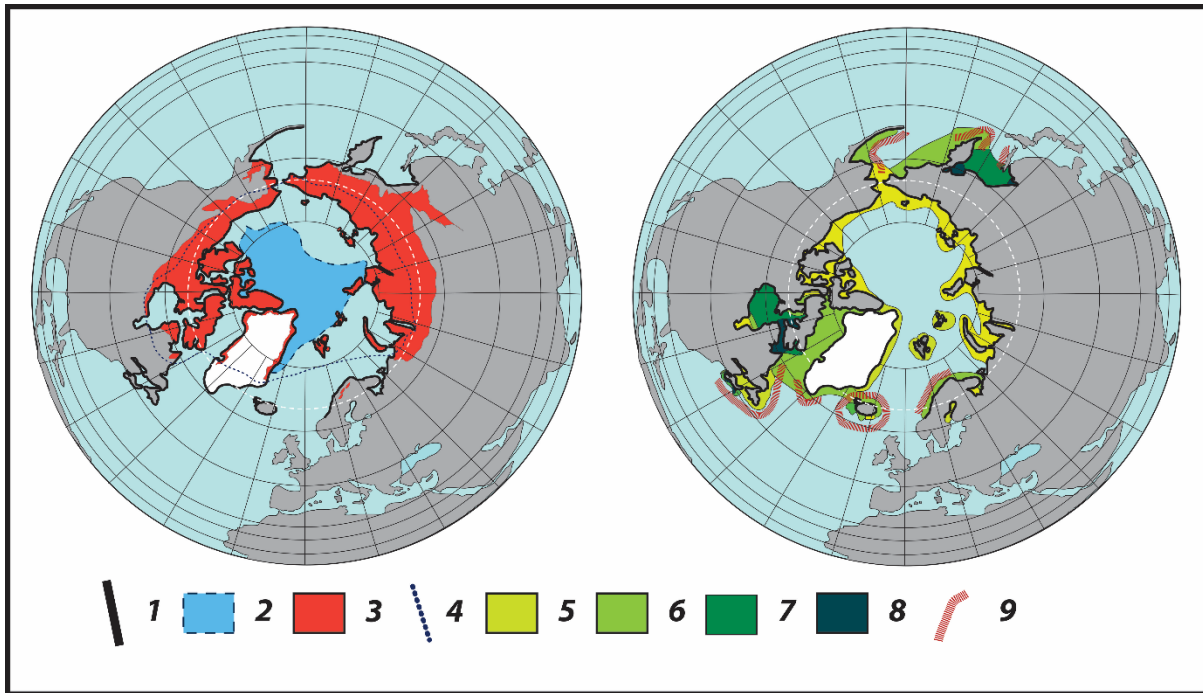
663 Węśławski, J.M. (ed.), 2011. Adventfjorden. Arctic sea in the backyard. Institute of Oceanology
664 PAS, Sopot, pp. 39.

665 Williams, R. B. G., Robinson, D. A., 1983. The effect of surface texture on the determination
666 of the surface hardness of rock using the schmidt hammer. *Earth Surface Processes and*
667 *Landforms* 8: 289–292.

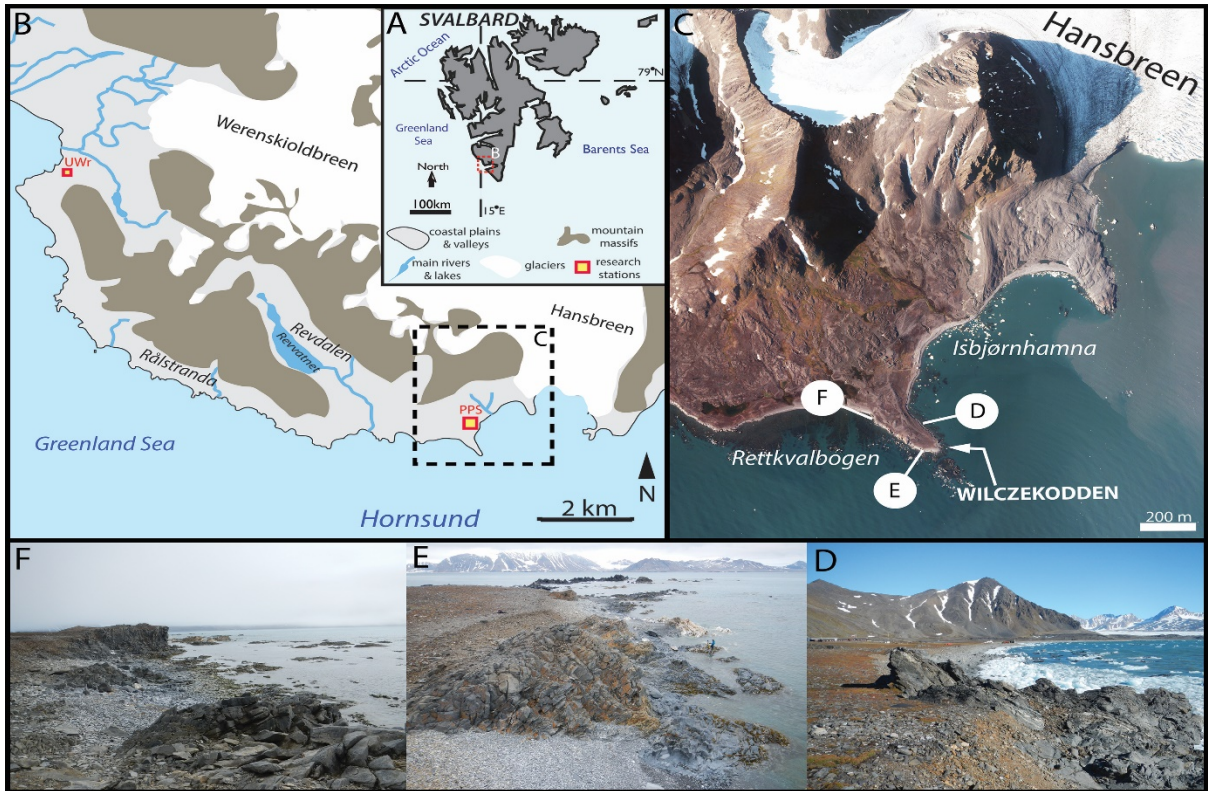
668 You, Y., Yu, Q., Pan, X., Wang, X., Guo, L. 2013. Application of electrical resistivity
669 tomography in investigating depth of permafrost base and permafrost structure in Tibetan
670 Plateau. *Cold Regions Science and Technology* 87, 19–26. 35.

671 Zagórski, P., Rodzik, J., Moskalik, M., Strzelecki, M.C., Lim, M., Błaszczuk, M., Promińska, A.,
672 Kruszewski, G., 2015. Multidecadal (1960–2011) shoreline changes in Isbjørnhamna
673 (Hornsund, Svalbard). *Polish Polar Research* 36: 369–390.

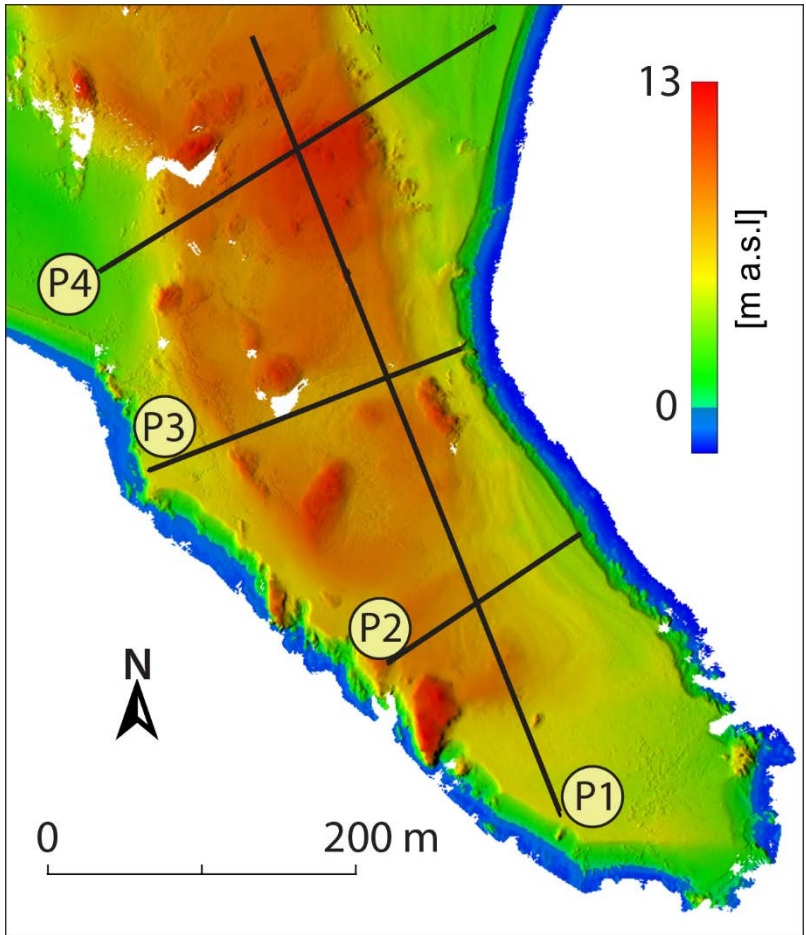
674



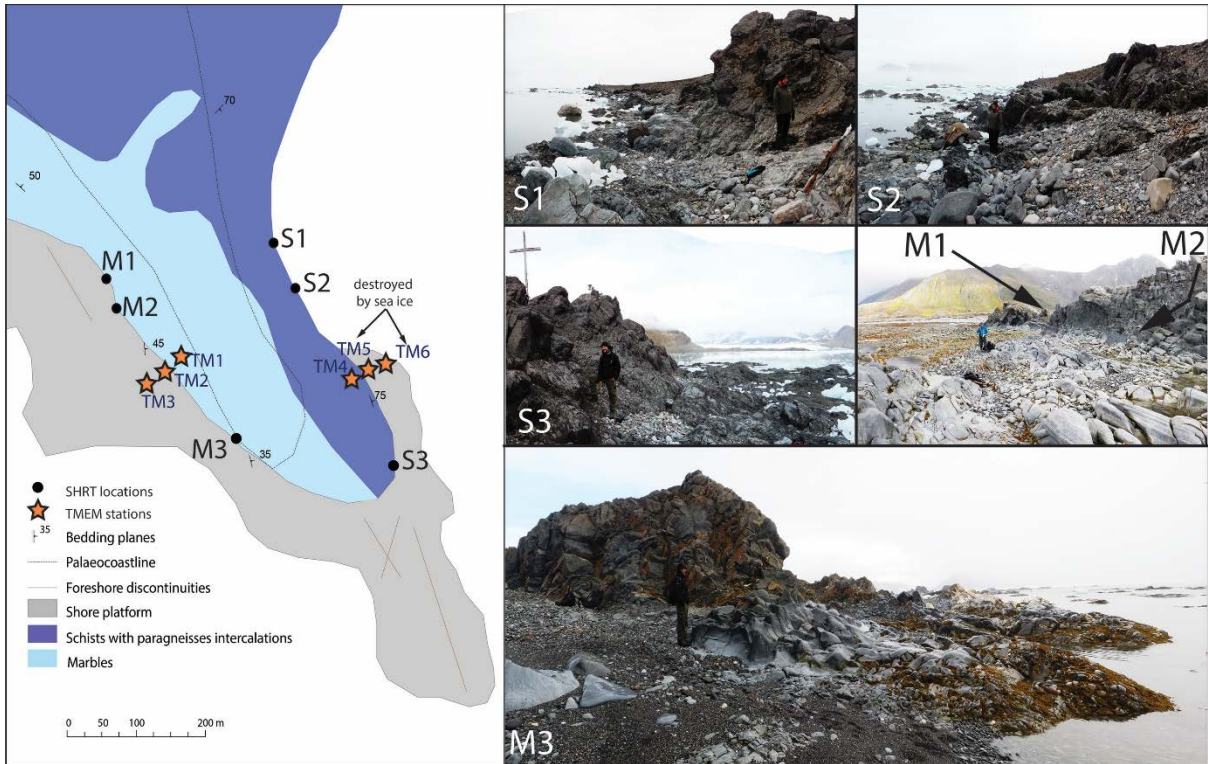
675
 676 Figure 1. Regional climatic and oceanographic factors controlling Arctic coastal
 677 geomorphology predicted to alter due to global warming and sea-level rise. 1 - cold region
 678 coasts according to Byrne and Dionne (2002) – defined as ‘areas where frost and ice processes
 679 are active during a period of the year, which is sufficient to have a significant, if not permanent,
 680 impact on the near terrestrial, coastal and marine environments’; 2 – minimum arctic sea ice
 681 extent in August 2016 (source: National Snow and Ice Data Centre: <http://nsidc.org/>); 3 - zone
 682 of continuous permafrost (source: National Snow and Ice Data Centre: <http://nsidc.org/>); 4 –
 683 zone of less than 60 frost-free days per year (after Davies 1980); Spring tidal range along cold
 684 region coasts (after Davies 1980): 5 – tides <2 m; 6 – tides 2-4 m; 7 – tides 4-6 m; 8 – tides
 685 >6 m; 9 – storm wave environments in cold regions (after Davies, 1980).
 686
 687
 688



689
 690 Figure 2. Location of study area A) Svalbard Archipelago; B) Entrance to Hornsund in
 691 southwestern part of Spitsbergen, largest island of Svalbard Archipelago; C) Wilczekodden –
 692 rocky cape near Polish Polar Station. Background aerial image taken by Norwegian Polar
 693 Institute in 2011; D) Eastern coast of Wilczekodden composed of shale. Cliff base, shore
 694 platforms and skerries are frequently impacted by icebergs and growlers resulting from calving
 695 of tidewater Hansbreen; E) Tip of Wilczekodden with well-developed shale and marble shore
 696 platforms, exposed to storm waves arriving from Greenland Sea; F) high cliffs and wide
 697 platforms along western coast of Wilczekodden.
 698
 699

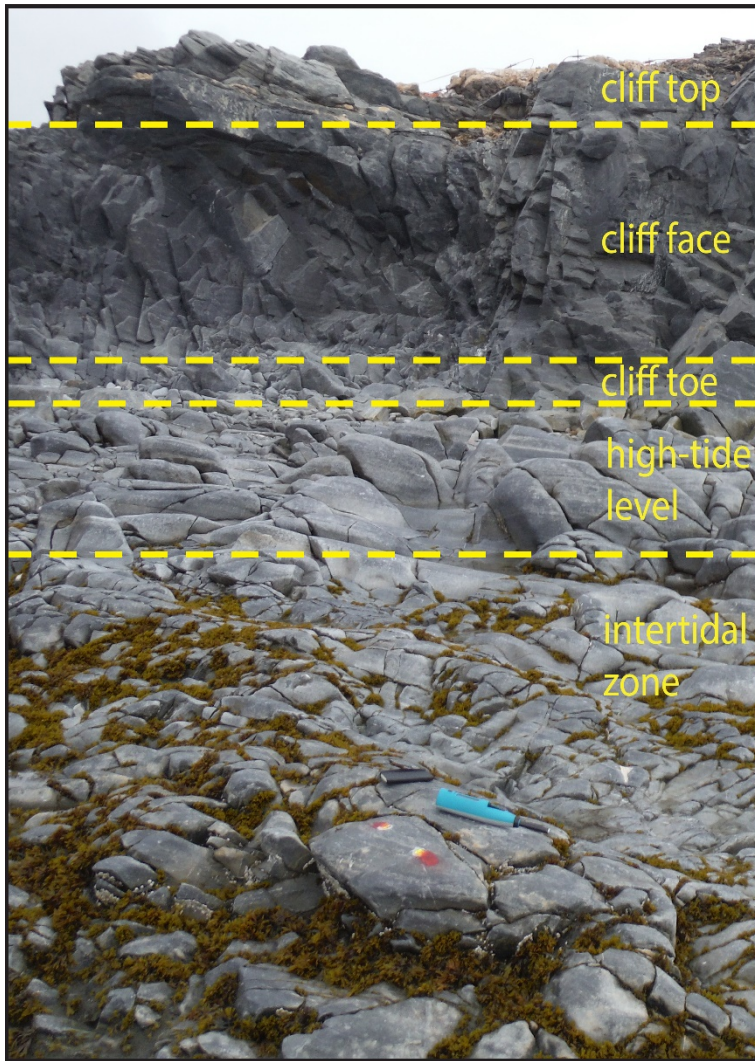


700
 701 Figure 3. Location of five ERT profiles : P1-P4 on Wilczekodden. Background – Digital
 702 Elevation Model based on terrestrial laser scanning in years 2015-2016.
 703
 704
 705

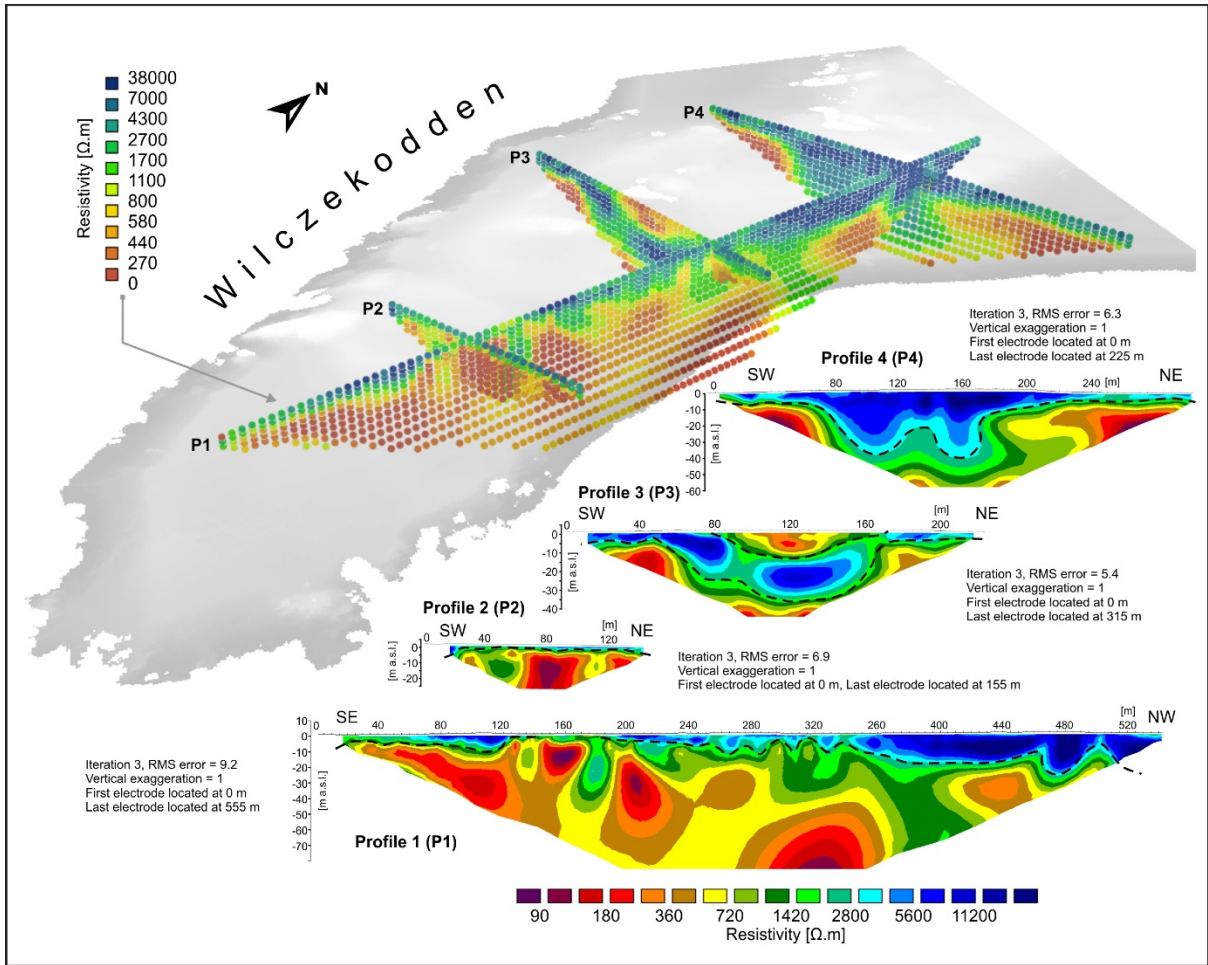


706
 707
 708
 709
 710
 711

Figure 4. Location of SHRT profiles (S1-S3 – schists; M1 –M3 marbles) and TMEM measurements sites (TM1-TM6). Background geological map of the study area modified from Czerny et al. (1992a).

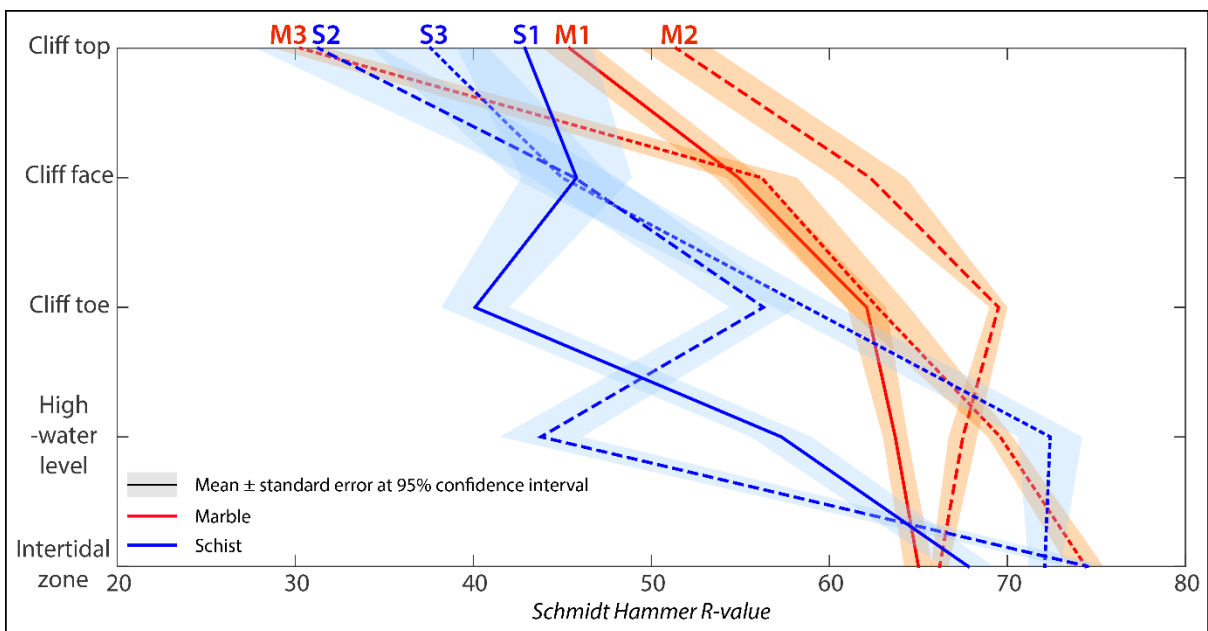


712
713 Figure 5. Five zones across the rocky shore profile from which SHRT measurements were
714 acquired. The photograph was taken at location M2 (author: Heather Bell, Durham
715 University).
716
717



718
719
720
721
722
723
724

Figure 6. Results of electrical resistivity tomography on Wilczekodden. Obtained inversion models (profiles P1–P4), imaging apparent resistivity of ground, are presented separately and as oblique view in combination with digital terrain model (greys). High values of resistivity (blue colours marked also by dotted lines) are interpreted as frozen ground.

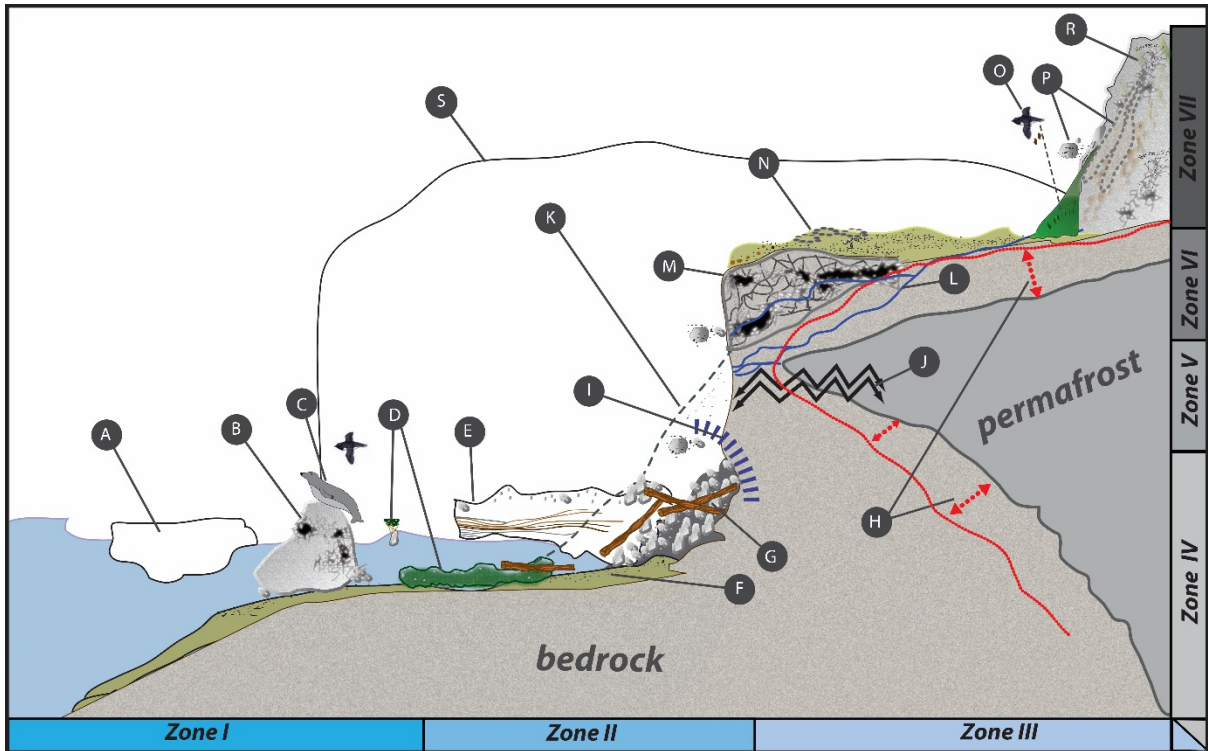


725

726 Figure 7. Schmidt hammer R-values at different elevational zones for six locations along the
727 coast of Wilczekodden, Hornsund, Svalbard.
728
729



730
731 Figure 8. Surface change rates observed in three TMEM stations installed across marble rock
732 coast, between 2nd of August 2015 and 21st of July 2016.
733
734
735



736
737

738 Figure 9 . Environmental factors controlling the functioning of High Arctic rock coasts: A - sea
739 ice action; B - glacial erratics/ boulders accumulations in the intertidal zone; C -
740 bioerosion/weathering of rock fragments in the intertidal zone; D - sediment transport and
741 protection by seaweeds; E- development of icefoot complex; F-accumulation/redistribution of
742 sediment cover on shore platforms; G- accumulations of driftwood, H – active layer
743 development including bottom active layer postulated by Kasprzak et al.(2016), I - upper limit
744 of storm wave action and sea spray extent, J - postglacial rock debuttresing, K -
745 snowdrift/avalanche derived deposits, L – groundwater and springs, M - karstic landforms and
746 processes (rock dependent) , N – uplifted marine deposits with various degrees of periglacial
747 sorting; O - vegetated slopes (fertilized by bird colonies). P- debris flows and rockfalls; R -
748 relict/uplifted rock coasts (cliffs and platforms). Zones I – VII refer to Table I.
749

750 Table I. Zonation of a High Arctic rock coast system based on mechanism controlling coastal zone development

High Arctic rock coast zone	Mechanisms
Zone I	<ul style="list-style-type: none"> • Seaward section of shore-platform, exposed during the low spring tides, subject to sea ice scouring and deposition of drop stones, affected by thermal changes in subsea permafrost.
Zone II	<ul style="list-style-type: none"> • Landward section of the shore platform, in summer months subject to tidal-dependent wetting-drying cycle as well as to operation of waves that redistribute sand-gravel sediments on the platform surface. The thickness, size and roundness of sediment covering the shore platform influence the efficiency of wave quarrying and the rate of rock surface polishing. Wave and tidal action is also responsible for driftwood and seaweed accumulations within the zone, which may have an impact on shore platform microrelief (Strzelecki, 2016). The degree of rock saturation is dependent on the development of an active layer which in this zone often occurs in a discontinuous form (e.g. Kasprzak et al., 2016). Saturated, often cracked rock surfaces are prone to disintegration due to freeze-thaw cycles. In winter, this zone is protected by an icefoot complex and thick snowdrifts (Strzelecki, 2016).
Zone III	<ul style="list-style-type: none"> • Inner part of the rocky outcrop bounded by permafrost and affected by post-glacial debuttreasing after retreat of glacier/ice stream filling the fjord during glaciation; potential to evolve into a new shore platform.
Zone IV	<ul style="list-style-type: none"> • Section covering the junction with the modern shore platform and cliff wall. Affected by tides, waves and sea spray with very diverse microrelief and often covered with halokarstic features (dependent on rock lithology). Subject to intensive wetting-drying during open-water months and intensive frost weathering during cooler months. Protected by icefoot complex and thick snowdrifts in winter (e.g. Jahn, 1961; Ødegård and Sollid, 1993; Ødegård et al., 1995);
Zone V	<ul style="list-style-type: none"> • Middle zone of the rockwall, which is not reached by waves and sea spray, affected by thermal changes in the permafrost bounding the inner section of outcrop and post-glacial rock debuttreasing (e.g. Wangenstein et al., 2007; Strzelecki, 2011). Rock shelves within this zone are often covered with debris. Summer thawing of active layer opens the network of karstic channels which often progress down the rockwall (Strzelecki, 2016). In winter months this zone is protected by sporadic snowdrifts.
Zone VI	<ul style="list-style-type: none"> • Top of the rocky cliff is often characterized by heavily weathered rock layers related to lack of the snow insulation and intensive biochemical weathering (particularly around bird colonies) as well as periglacial weathering (e.g. Strzelecki, 2011; Strzelecki, 2016). Often covered with uplifted marine deposits and debris/rock falls from surrounding talus slopes, drift-mantled slopes and mountain slopes (e.g. Kasprzak et al., 2016).
Zone VII	<ul style="list-style-type: none"> • Section of relict cliffs and shore platforms currently reshaped by operation of periglacial and paraglacial geomorphic processes (e.g. Migoń, 1997).

751

752

753